Progress in Organic Coatings 90 (2016) 44–53

Contents lists available at ScienceDirect

Progress in Organic Coatings

journal homepage: www.elsevier.com/locate/porgcoat

Characterisation of commercially CVD grown multi-walled carbon nanotubes for paint applications

Christopher M. White[a,b,*], Richard Banks[b], Ian Hamerton[c,1], John F. Watts[a]

[a] Department of Mechanical Engineering Sciences, University of Surrey, Guildford, Surrey GU2 7XH, UK
[b] Indestructible Paint Ltd, Birmingham B11 3TA, UK
[c] Department of Chemistry, University of Surrey, Guildford, Surrey GU2 7XH, UK

ARTICLE INFO

Article history:
Received 4 February 2015
Received in revised form
17 September 2015
Accepted 22 September 2015

Keywords:
Carbon nanotubes
Surface analysis
Electron microscopy
Raman spectroscopy

ABSTRACT

Commercially grown, multi-walled carbon nanotubes (MWNTs), available in kilogram quantities from three commercial suppliers have been characterised using a number of analytical techniques. The catalysts used in the growth of the MWNTs are identified by energy dispersive X-ray spectroscopy (EDX) and different growth mechanisms are postulated to explain the various structures present in the MWNT stock in its as-supplied form. A tightening of the agglomerate structures during purification and functionalisation is shown using scanning electron microscopy (SEM) and confirmed more qualitatively using pore-size distributions obtained using the Brunauer–Emmett–Teller (BET) method and non-local density functional theory (NLDFT) calculations. Differences in thermal stability are shown using thermogravimetric analysis (TGA) and are related back to the residual catalysts present. X-ray photoelectron spectroscopy (XPS) is used to confirm functionalisation of certain grades and Raman spectroscopy is used to investigate the level of defects present.

1. Introduction

Multi-walled carbon nanotubes (MWNTs) have received much interest since they were brought to the attention of the wider research community in 1991 by Iijima [1] and although commercially available, have yet to become widely utilised by industry in large volume applications. MWNTs have extraordinary mechanical [2], electrical [3] and thermal [4] properties and are now being used in many research areas and commercial products; ranging from coatings [5–7] and composites [2,8,9] to batteries [10–12] and filters [13]. This work is part of a wider programme to assess the potential of MWNTs as pigmentation for matt black static dissipative coatings for the aerospace industry. For this reason it has been important to assess the characteristics of a selection of MWNTs that are available in kilogram quantities, at prices that would not make the cost of the end product prohibitively expensive. Although there are papers addressing the characterisation of various grades of MWNTs [14,15], there is a need for the characterisation of a wider range of commercially grown MWNTs using the same characterisation methodology.

In this study MWNTs, commercially grown via chemical vapour deposition (CVD) methods by Nanocyl™, Arkema and Bayer MaterialScience, are comprehensively characterised by scanning electron microscopy (SEM), energy dispersive X-ray spectroscopy (EDX), X-ray photoelectron spectroscopy (XPS), Raman spectroscopy, thermogravimetric analysis (TGA), surface area analysis by the Brunauer–Emmett–Teller (BET) method and pore size distributions (PSDs) using non-local density functional theory (NLDFT). This characterisation will aid in the formulation of coatings and composites using MWNTs where attributes such as agglomerate structure and surface area affect the optimum dispersion method, processing time and dispersant loading.

MWNTs are not only available in their raw state and are often used in a purified or functionalised state. The most common purification and functionalisation methods for MWNTs involve further wet processing in acids [16,17] and length reduction of MWNTs has been achieved in various ways including oxidation with acids [18] and ball milling [16,19]. All of these techniques involve wet processing followed by washing and then drying of the nanotubes; in this study the restructuring of the MWNT agglomerates after processing is evaluated.

The most basic industrial coatings are a fluid blend of binder, solvents, additives and pigments. The inclusion of MWNTs into a

* Corresponding author. Current address: GKN Aerospace Services Ltd, Golf Course Lane, Bristol BS34 9AU, UK.
E-mail address: Chris.White@GKNAerospace.com (C.M. White).
[1] Current address: The Advanced Composites Centre for Innovation and Science, University of Bristol, Bristol BS8 1TR, UK.

http://dx.doi.org/10.1016/j.porgcoat.2015.09.020

coating can introduce electrical conductivity, physical reinforcement and other properties to the coating. These properties have a high dependency on the MWNTs remaining reasonably untangled and uniformly dispersed during storage and coating curing. All of these properties are directly influenced by the physical properties of the MWNTs that are investigated within this study.

2. Materials

MWNTs were sourced from Nanocyl™ S.A. (Belgium), Arkema (France) and Bayer MaterialScience AG (Germany). Details of the various grades are summarised in Table 1 along with properties as detailed in the suppliers' technical data sheets [20–25].

3. Techniques

SEM was performed on a JEOL JSM-7100F field emission SEM equipped with a Thermo Scientific triple analysis system featuring an UltraDry EDX detector, used in this work, a MagnaRay wavelength dispersive X-ray (WDX) system and a QuasOr camera for electron backscatter diffraction (EBSD). An accelerating voltage of 8 kV was employed for SEM images and 15 kV for EDX analysis. For SEM, samples of each MWNT powder were sprinkled onto carbon adhesive tabs and a 2 nm gold coating was applied to reduce charging effects. For X-ray analysis, samples of each MWNT powder were sprinkled onto a fragment of silicon wafer. Three locations from three separate agglomerates were analysed by EDX for each MWNT sample at a magnification of 5000×. The mean result was then used to confirm the elements present. The substrate signal (SiKα) was excluded from the quantification.

XPS was performed using a Theta Probe spectrometer (Thermo Scientific) operating in constant analyzer energy (CAE) mode using a monochromated Al-Kα anode. Survey spectra were obtained from 0 to 1350 eV using a pass energy of 300 eV and a step size of 0.4 eV. High resolution spectra of the C1s, O1s and, where appropriate, N1s, Ca2p and Cl2p regions were obtained using a pass energy of 20 eV and a step size of 0.2 eV. Quantitative surface analysis was calculated from the high resolution core level spectra by peak fitting, following the removal of a non-linear Shirley background, using the manufacturer's standard *Avantage* software.

Raman spectroscopy was performed on a Reinshaw inVia micro-Raman spectrometer with a laser wavelength of 633 nm and a power of 1.67 mW measured at the sample. A 50× objective was used and the scan time of 10 s. Ten spectra were collected from different agglomerates for each MWNT sample. Peak fitting was performed using Origin Pro software.

TGA was performed on a TA Q500 (TA Instruments) from room temperature to 800 °C with a heating rate of 5 °C/min. The sample size was ca. 5 mg and the analysis was performed in air, and a balance gas of nitrogen, with flow rates of 60 ml/min and 40 ml/min respectively.

Nitrogen adsorption isotherms were measured using a Gemini V surface area analyser (Micromeritics) at 77 K. Specific surface areas (SSA) were calculated using the BET method [26] and the PSDs were calculated using the infinite slit NLDFT model [27,28] on the adsorption isotherm. The analysis software used was *DataMaster* from Micromeritics. Before analysis, samples were out-gassed under N_2 for 24 h at 150 °C using FlowPrep 060 (Micromeritics).

4. Results and discussion

4.1. Appearance by SEM

Low magnification SEM micrographs reveal differences in the MWNT agglomerates that make up the supplied powder. NC7000 consist of ropes or yarns, ca. 2–3 μm in diameter, of highly entangled tubes showing some degree of alignment. These ropes then tangle to form larger, more loosely entangled agglomerates ranging in size from ca. 10 μm to 1 mm, individual ropes up to 40 μm in length from support to tip were observed. Both C150P and C100 resemble more 'birds-nest' type agglomerates showing no sign of ropes or alignment. These tubes are also highly entangled, with agglomerate dimensions in the same range as NC7000, but with the majority towards the higher end of the scale, with C100 being most consistent in size. SEM micrographs showing typical agglomerates from each sample are shown in Fig. 1.

For samples that have undergone further processing, such as purification, shortening or functionalisation, the agglomerate structure changes, as shown in Fig. 2. Nanocyl™ NC3100, a purified grade based of NC7000 appears to have similar sized agglomerates and still has signs of a rope structure, although these are much less clear than in NC7000 agglomerates, and the individual tubes seem more tightly entangled. NC3101, a carboxylic acid functionalised grade based on NC3100, appears to have a similar structure to NC3100, although the tightening of the agglomerates seems even more severe. NC3151, a shortened and then acid functionalised grade based on NC3100, consists of much smaller primary agglomerates and again, the individual tubes are even more tightly tangled together. Bayer C150HP, a purified grade of C150P, follows a similar change as that from NC7000 to NC3100 in that the agglomerates seem similar in size, but the entanglement has tightened.

Based on these observations there is an indication that wet processing steps lead to a tightening of nanotube agglomerates and that the process Nanocyl™ use to shorten their MWNTs leads to a reduction in agglomerate size.

4.2. Bulk composition by EDX

It is well known that most MWNTs carry a small concentration of catalyst residue within their structure. EDX was used to determine the composition of the metal catalysts used in the synthesis of the MWNTs and to identify any contaminants present. The spectra obtained for NC7000 is shown in Fig. 3, catalysts residues are readily observed with an intense AlKα signal and weak signals of FeKα and CoKα.

Table 1
A Summary of the MWNTs investigated and properties supplied by the manufacturers.

Product name	Description	Quantity (g)	C purity (%)	Diameter (nm)	Length (μm)
Nanocyl™ NC7000	Industrial grade	2000	90	9.5	1.5
Nanocyl™ NC3100	Purified grade	2	>95	9.5	1.5
Nanocyl™ NC3150	Purified and shortened	2	>95	9.5	<1
Nanocyl™ NC3101	Purified and COOH functionalised grade	2	>95	9.5	1.5
Nanocyl™ NC3151	Purified, shortened and COOH functionalised grade	2	>95	9.5	<1
Nanocyl™ NC3152	Purified, shortened and NH_2 functionalised grade	2	>95	9.5	<1
Arkema C100	Industrial grade	100	>90	10–15	0.1–10
Bayer C150P	Industrial grade	500	>95	5–20	1–10
Bayer C150HP	Purified grade	1000	>95	5–20	1–10

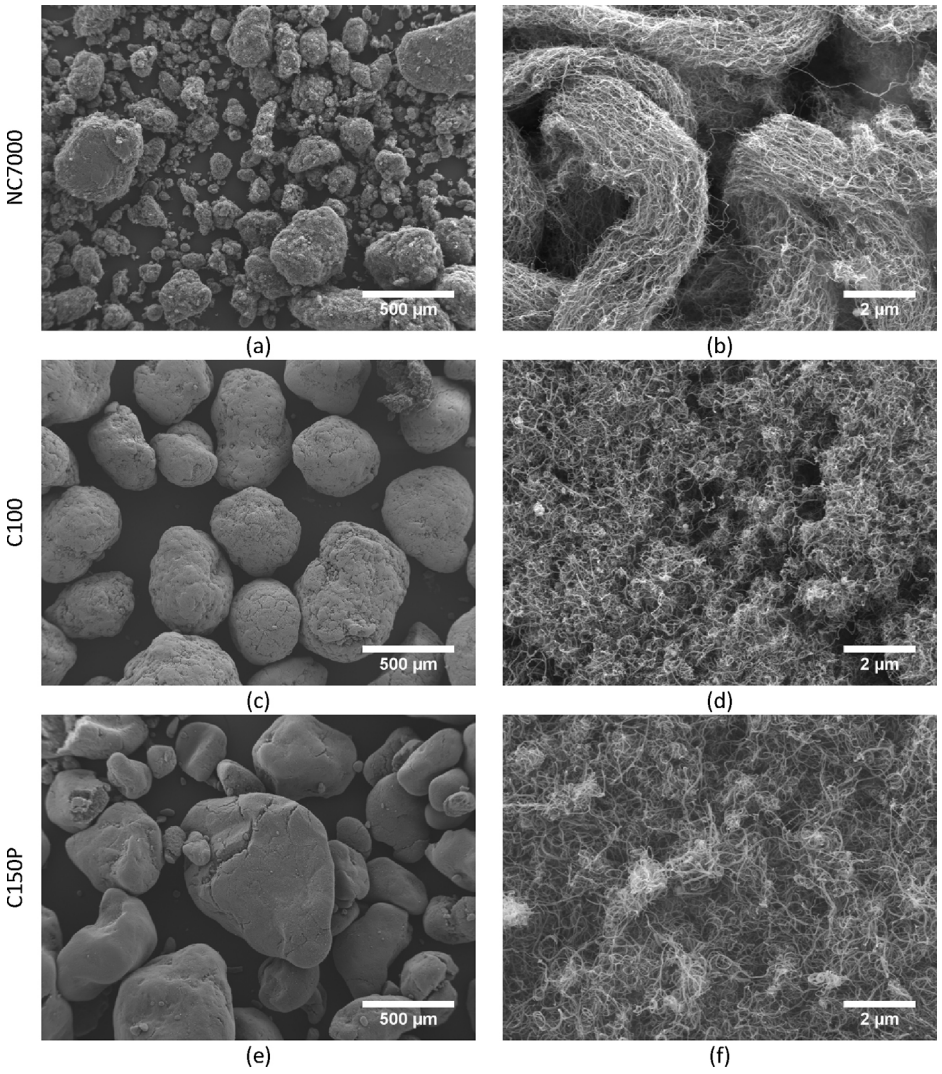

Fig. 1. SEM micrographs showing the agglomerate size and structure of the industrial grade MWNTs; NC7000 (a, b), C100 (c, d) and C150P (e, f).

Table 2
EDX analysis of the MWNT powders.

	Main impurities (wt%)	Trace impurities
NC7000	Al (5.9) Fe (0.5) Co (0.2)	Na
NC3100	Fe (0.2 Co (0.1)	
NC3150	Al (0.1) Fe (0.2) Co (0.1)	Ca Cl S Mg
NC3101	Fe (0.5) Co (0.1) Cl (0.9) Mg (0.3) Ca (2.6) Mn (0.1)	Al Na S
NC3151	Al (0.1) Fe (0.2) Cl (2.4) Mg (0.3) Na (0.1) Mn (0.4) Ca (1.5)	Co S K
NC3152	Al (0.1) Fe (0.6) Co (0.3) Cl (0.2) Ca (0.2)	Na Mg S
C100	Al (1.2) Fe (4.5)	
C150P	Al (0.5) Mg (0.5) Mn (0.5) Co (0.5)	
C150HP	Co (1.2) Cl (0.3)	Al Mn

Table 2 summarises the elements detected for each CNT powder. All quantities are based on the mean analysis of three separate area scans on three different agglomerates. Only elements detected in all three analysis areas are shown as main impurities, with mean values higher than 0.1% by weight. It should be noted that some elements are present very close to the sensitivity limit of EDX and that the samples were not flat or dense, making them less than ideal samples for EDX analysis. NC7000 shows a large amount of aluminium and smaller quantities of both iron and cobalt. C150P contains mainly cobalt, manganese, magnesium and aluminium and C100 mainly iron and aluminium. MWNTs are routinely grown from iron, cobalt and manganese catalysts and aluminium oxide and magnesium oxide are used as catalyst supports [29–32], which explains the presence of these elements. These elements are also mentioned in various patents from Nanocyl™ [33,34], Bayer MaterialScience [35,36], and Arkema [37].

When purified to NC3100 the large quantity of aluminium oxide present in NC7000 reduces to just trace amounts, as does the cobalt concentration. Traces of sulphur are also present, indicating that the purification step used by Nanocyl™ probably involves the use of sulphuric acid. Purification of both Nanocyl™ and Bayer industrial grades results in a large reduction in catalyst and catalyst support, but appears more effective at removing the support than the metal catalyst particles; thereby indicating some catalyst may be located inside the nanotubes, as reported by Pumera [38]. Nanotubes that have undergone further processing contain additional contaminants including chlorine, sulphur, calcium and magnesium.

EDX elemental mapping shows the distributions of the metal catalysts and catalyst support within the agglomerates and the results for the three industrial grades are shown in Fig. 4. The overlapping of the oxygen and aluminium atoms confirms the support material for all three industrial grades and iron (NC7000 and C100) and cobalt (C150P) maps confirm the finely dispersed catalyst particles.

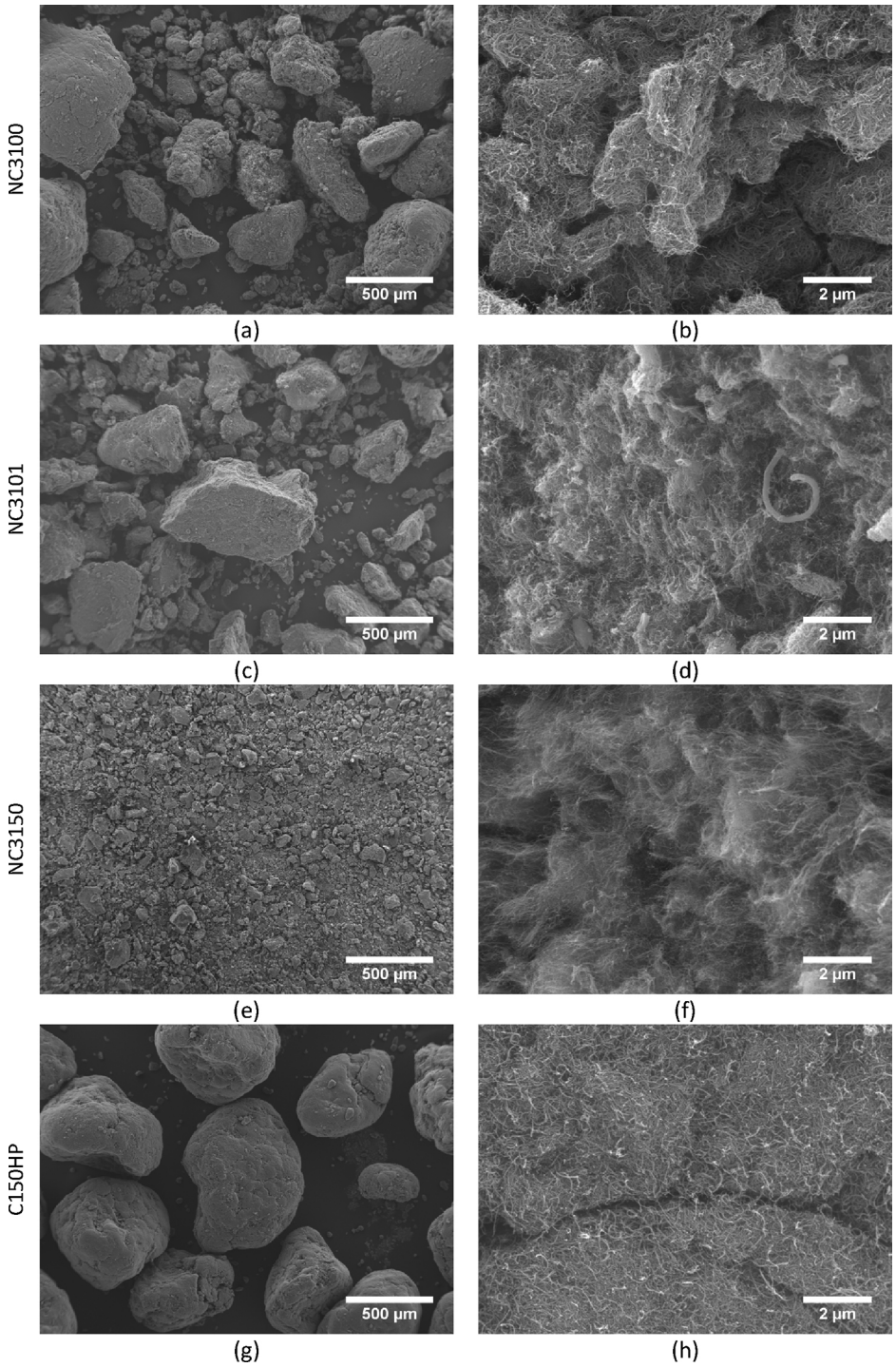

Fig. 2. SEM micrographs for NC3100 (a, b), NC3101 (c, d), NC3150 (e, f) and C150HP (g, h) showing changes in agglomerate structure.

A good review of nanotube growth is given by Zhang et al. [39] who divided nanotube growth into two types; either aligned or agglomerated. Typical powder catalysts used in nanotube synthesis consist of metal nanoparticles on a support. When a source of carbon is introduced (for example methane), carbon nanotubes grow and as they grow they crush and eventually rupture the catalyst particles, dispersing them throughout the nanotube agglomerate that is formed. This is the method of growth used to produce Baytubes® [40] and explains the 'birds nest structure' observed by SEM and the finely dispersed catalyst seen in the EDX maps for Bayer C150P (Fig. 4). As the SEM micrographs and EDX maps for C100 are very similar to C150P, it is likely they also grow in this way. Nanocyl™ NC7000 contains distinctive support particles of aluminium oxide which have not been crushed and finely dispersed throughout the agglomerates and the EDX maps show ropes growing from both sides of these well defined support particles, making them very different from both C100 and C150P. The SEM micrograph and EDX maps shown in Fig. 5 clearly show the primary structure of NC7000 as highly entangled ropes grown from an aluminium oxide support. The highly entangled nature of the ropes may be explained by the surface of the aluminium oxide support; Atthipalli et al. [41] showed that the surface roughness of the

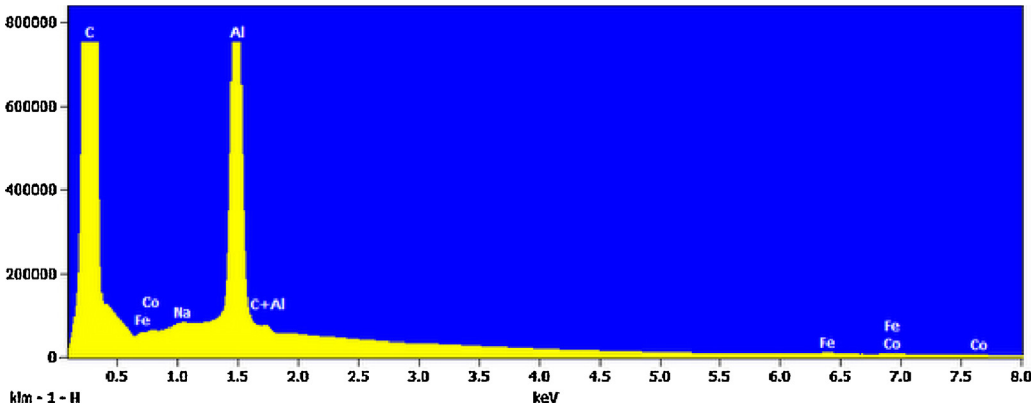

Fig. 3. EDX spectra for NC7000.

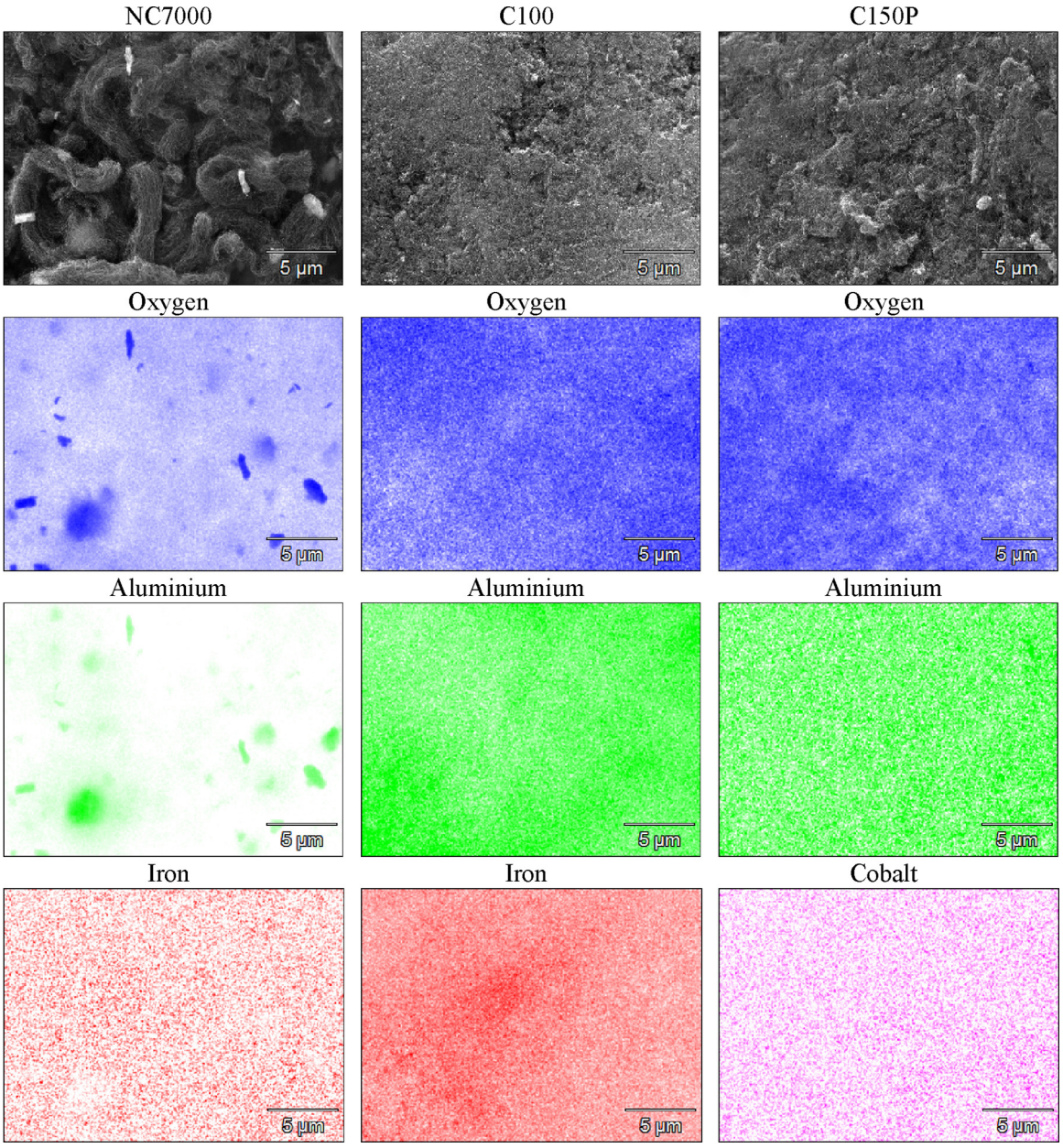

Fig. 4. EDX elemental maps for the three industrial grades of MWNTs.

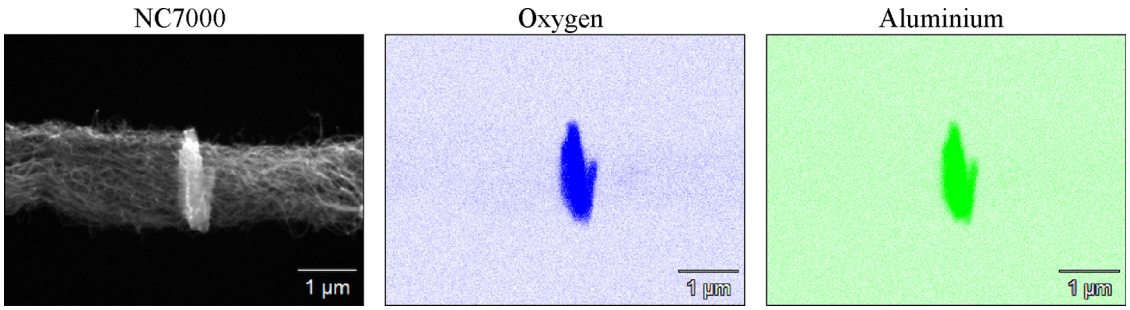

Fig. 5. EDX elemental maps showing the ropes of NC7000 clearly growing from aluminium oxide particles.

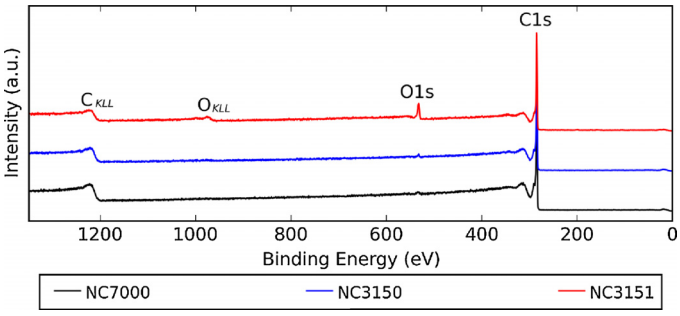

Fig. 6. XPS survey spectra for various grades of MWNTs.

support used to grow carbon nanotubes reduces alignment and a patent from Nanocyl™ [33] describing catalyst production refers to milling and sieving of support powder that would not lead to a smooth surface.

4.3. Surface analysis by XPS

XPS reveals the surface chemistry of the MWNTs. The survey spectra for NC7000, NC3150 and NC3151 are shown in Fig. 6. The degree of graphitisation and oxidation can be measured using the C1s peak and O1s peak, respectively.

The spectra are dominated by the C1s peak at 284.8 eV with a small O1s peak at 532 eV that increases and broadens in the acid functionalised grades. The O1s peak at 532 eV corresponds to the carbonyl bond in an acid or ester [42,43]. The results of the quantitative surface analysis are summarised in Table 3.

All MWNT grades have oxygen on the surface, likely as a result of the catalytic growth process; the quantity of oxygen is relatively low in the raw industrial grades, although for NC7000 is slightly higher than C100 and C150P. While this could be a result of the high level of aluminium oxide in NC7000, aluminium was not detected by XPS. There is no increase in oxygen when comparing NC7000 to NC3100, which would indicate that the purification process used by Nanocyl™ does not impact the degree of oxidation of the nanotubes. Shortening of the MWNTs may increase the degree of oxidation of the MWNT, which is expected as the tubes are broken, but this cannot be shown definitively as any small increase or decrease could be from batch-to-batch variation. For the acid functionalised grades from Nanocyl™, there is a clear increase in oxygen surface concentration to 11.6% and 12.9% for purified and purified-shortened grades respectively, confirming the addition of oxygen containing groups on the nanotube surface.

Table 3
Surface chemical analysis of the MWNT powders.

	Surface composition (atomic%)				
	C	O	N	Cl	Ca
NC7000	98.5	1.5	–	–	–
NC3100	98.8	1.6	–	–	–
NC3150	97.7	2.3	–	–	–
NC3101	87.9	11.6	–	–	0.6
NC3151	86.8	12.9	–	0.3	–
NC3152	98.0	1.4	0.6	–	–
C100	99.5	0.5	–	–	–
C150P	99.2	0.8	–	–	–
C150HP	97.7	2.3	–	–	–

4.4. Raman spectroscopy

Raman spectroscopy is widely used to provide information relating to the quality of nanotubes, although most work relates to single walled nanotubes with MWNTs being less well understood. The main features of a Raman spectra for a graphitic material are described in detail by Dresselhaus et al. [44] and Farrari et al. [45] but for MWNTs the spectra consist mainly of the D band (≈1350 cm^{-1}), G Band (≈1580 cm^{-1}), and 2D (≈2700 cm^{-1}) band, sometimes called G′ band. The disorder induced D band relates to vibrations from defects present in a carbon structure. The G band relates to the in-plane vibration of an ideal sp^2 bonded carbon structure and the 2D band is the first overtone of the D band and is always present in a graphitic sample and is used to infer long range order in a carbon based structure.

The ratio of I_D/I_G has long been used as an indication of the quality of nanotubes with an increase in the ratio, meaning more defective nanotubes or the presence of more amorphous carbon in the sample. Behler et al. [46] observed a change in the position and intensity of the D band with changing excitation wavelength, making it difficult to standardise and compare I_D/I_G ratios obtained using different wavelengths. DiLeo et al. [47] proposed that defects would reduce the double resonance process that results in the decreasing of the 2D band, making the I_{2D}/I_G ratio a better indicator of crystalinity in MWNTs. Another advantage to using the 2D band, as opposed the D band, is that the 2D band is always present and satisfies the Raman selection rule [48] where the D band is forbidden and requires defects to be present [49]. Other researchers have used the ratio of the areas of the peaks rather than the intensities to infer quality [50].

Fig. 7 shows a typical Raman spectra for NC7000 with a relatively intense D band and a G band of lower intensity, typical of a highly defective structure [51].

Table 4 summarises the ratios of the intensities as peak heights (I) and areas (A) of the D band to G band and the 2D band to the G band.

All ratios are similar to each other, with only C100 showing a slightly lower D/G band ratio and slightly higher 2D/G band ratio, inferring lower numbers of defects and higher crystallinity. As discussed, it can be difficult to directly compare Raman spectra and thus band ratios obtained using different equipment, but these similarities are in agreement with Tessonnier et al. [14] who showed NC3100 and C150P had similar I_D/I_G ratios of 2.1 and 1.8,

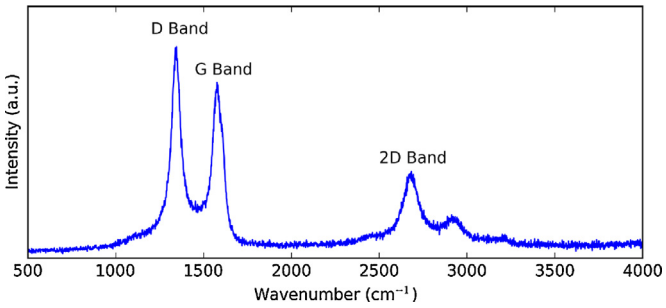

Fig. 7. Typical Raman spectra for NC7000.

Table 4
Intensity and area ratios for Raman peaks.

Sample	I_D/I_G	I_{2D}/I_G	A_D/A_G	A_{2D}/A_G
NC7000	1.12	0.45	1.24	0.79
NC3100	1.11	0.42	1.27	0.77
NC3150	1.08	0.43	1.21	0.79
NC3101	1.14	0.41	1.23	0.70
NC3151	1.17	0.36	1.27	0.67
NC3152	1.09	0.42	1.25	0.76
C100	0.93	0.61	1.02	1.02
C150P	1.09	0.51	1.17	0.87
C150HP	1.12	0.46	1.21	0.79

respectively. Due to the similarity of the D/G band and 2D/G band ratios, it can be concluded that the purification processes used by both Nanocyl™ and Bayer MaterialScience and the functionalisation process used by Nanocyl™ do not increase the number of defects within the nanotubes.

4.5. Surface area and pore size distribution

SSA is an important parameter for a pigment as it provides an indication to the amount of binder, or dispersant, that is required to fully wet the particle surface. The pore size distribution was investigated to detect the differences in agglomerate structure observed via SEM.

All nanotubes exhibit Type IV BET isotherms with Type II characteristics, according to the IUPAC classification [52,53]. This indicates a mesoporous material with possible small macropores. Isotherms for various Nanocyl™ grades are shown in Fig. 8.

The SSA and total pore volume for each nanotube powder are summarised in Table 5.

Industrial grade nanotubes from Nanocyl™ have the highest SSA at 475 $m^2 g^{-1}$ followed by Arkema with 249 $m^2 g^{-1}$ and lastly Bayer with 210 $m^2 g^{-1}$. Peigney et al. [54] showed that nanotube surface area was related to nanotube diameter and number of walls and this is likely the source of the difference between these samples. This is in agreement with the manufacturers data, showing C100

Table 5
SSA and total pore volume for the nanotube agglomerates showing nanotubes from Nanocyl™ have a higher surface area and pore volume than those produced by Arkema and Bayer.

	SSA ($m^2 g^{-1}$)	Pore volume ($cm^3 g^{-1}$)
NC7000	476	3.56
NC3100	323	2.86
NC3150	416	1.89
NC3101	317	1.17
NC3151	377	1.29
NC3152	318	1.45
C100	249	2.51
C150P	210	2.07
C150HP	221	1.67

and C150P having similar diameters and numbers of walls. The similarity in diameter was confirmed by Rosca et al. [8]. Nanocyl™ report a narrower diameter for NC7000, but do not specify this as the external diameter [20]. Tessonnier et al. [14] measured the SSA of NC3100, which are based on NC7000, and found it to be significantly higher than C150P and also observed that C150P had more wall terminations and more regular closing of the internal channels, drastically reducing the accessible internal surface area and thus explaining the higher SSA measured for NC7000 in this study. The SSA for NC3100 measured in this study was very similar to the 334 $m^2 g^{-1}$ measured by Tessonnier et al. but the SSA of C150P measured in this study is lower than the 228 $m^2 g^{-1}$ measured by Tessonnier et al. This is likely due to batch-to-batch variation, as an increased amount of residual catalyst would lead to an overestimation of the SSA of a MWNT sample. The residual catalyst measured by Tessonnier et al. using TGA for C150P was 4% compared to 2.9% in this study, which would account for the higher SSA.

When comparing Nanocyl™ purified MWNTs to their industrial grade equivalent, there is a reduction in SSA from 476 $m^2 g^{-1}$ to 323 $m^2 g^{-1}$ for NC7000 and NC3100, respectively. This decrease is likely due to either the removal of the catalyst support, which will have had a high surface area, or batch variation. Purified and shortened MWNTs from Nanocyl™ (NC3150) have a higher surface area than purified MWNTs, which is due to the shortening of the tubes making the internal channels within the tubes more accessible. The small increase in SSA when comparing C150P to C150HP, which has undergone a purification process, could be for the same reason. The functionalised grades from Nanocyl™ have lower SSAs than their un-functionalised equivalents, but they still show the same rise in SSA when the tubes are shortened.

The PSD for the industrial grade MWNTs are shown in Fig. 9 and show a bi-modal distribution. The first distribution (3–20 nm) falls within the diameter dimensions for the MWNTs when considering inner tube diameter, inner channel diameter and outer tube diameter and likely corresponds to pores attributed to individual tubes. The second distribution corresponds to spaces between tubes and is a result of the bundled nature of the nanotube agglomerates.

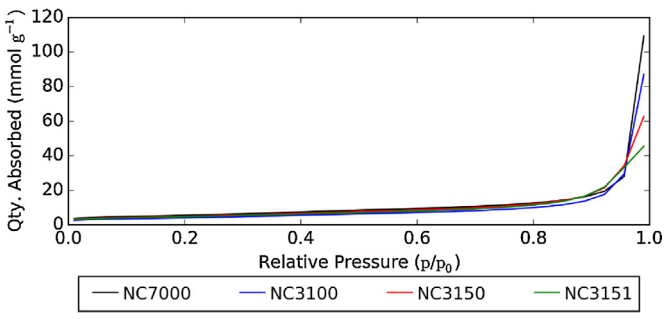

Fig. 8. BET adsorption isotherms for the Nanocyl™ range of MWNTs.

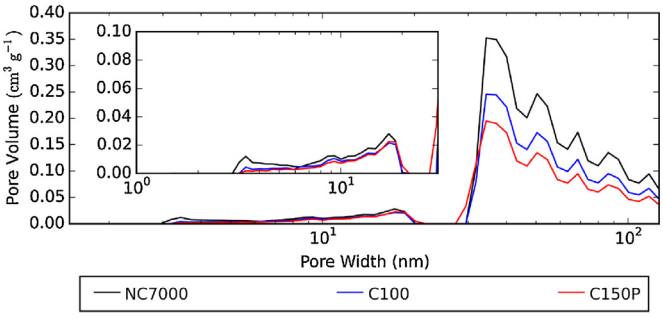

Fig. 9. PSDs for industrial grade MWNTs showing similar bi-modal distributions.

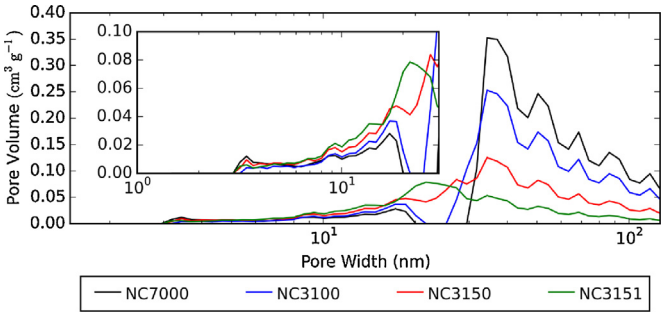

Fig. 10. PSDs for the various grades of MWNTs from Nanocyl™ showing a reduction in pore size with increased processing.

If the pore volume contributions are separated in relation to these distributions, an insight into the pore volume from within the tubes and from the agglomerates can be achieved.

Taking the Nanocyl™ range as an example, Fig. 10 shows a clear shift in the second distribution towards smaller pores after the nanotubes have been purified, shortened and functionalised, indicating a restructuring in the agglomerates in agreement with the observation from the SEM micrographs. The most common purification methods involve acid solutions [16,17], indicating the tubes are wet-processed and subsequently dried, which would explain this change in the agglomerate structure. For shortened tubes this change is even more pronounced and the shift leads to a combining of the two distributions, which is due to shorter tubes being able to pack more densely. Functionalisation, which involves further processing, follows this trend and the distributions not only combine but also shift even further towards smaller pores in the shortened grades.

Fig. 11 shows the cumulative pore volume for the two pore size ranges, for the MWNTs considered in this work. The volume in the pores with diameters <20 nm remains relatively consistent across nanotube samples, although there is an increase from NC7000 to NC3150, which again can be attributed to either tube opening or enlargement of defects. The same rise is present for NC3151 and NC3101, but not in NC3100, implying that the functionalisation process opens the tube ends or enlarges defects regardless of whether the tubes have been shortened or not. This same increase is observed when comparing C150P and C150HP, indicating either tube opening or defect enlargement or a combination of the two during Bayer's purification process. When considering the cumulative volume from larger pores in the agglomerate structure, it is clear that with increased processing steps, pore volume drops considerably. This is true for both Nanocyl™ and Bayer grades and shows the tightening of the agglomerates reducing the volume between the tubes, in agreement with SEM micrographs. Using this method to evaluate how tightly entangled agglomerates are, the PSD data indicate that NC7000 is more loosely agglomerated than C100, which is more loosely agglomerated than C150P, in agreement with Krause et al. [15] who found C150P required five times more energy to disperse than NC7000. In contrast, Tessonnier et al. [14] predicted that C150P was more loosely agglomerated than NC3100, which is based on NC7000, as less volume from larger pores was present. It is worth noting that NC7000 has two agglomerate structures; primary tightly agglomerated ropes and more loosely agglomerated bundles of ropes. The pore size distribution is an amalgamation of these two structures.

Table 6
Residual catalyst (as a% of initial mass), T_{50} and T_{MAX} of the MWNT powders.

	Residual (%)	T_{50} (°C)	T_{MAX} (°C)
NC7000	11.9	569	579
NC3100	2.5	585	598
NC3150	2.5	575	588
NC3101	4.7	472	498
NC3151	4.3	485	508
NC3152	2.8	558	571
C100	9.2	565	573
C150P	2.9	532	543
C150HP	1.8	566	581

4.6. Thermogravimetric analysis

TGA is often used to characterise the oxidation behaviour of MWNTs, as well as in the determination of the residual catalyst content [16,17,19,55]. Table 6 summarises the minimum residual catalyst for each sample after 800 °C; the temperature to 50% mass (T_{50}) and the temperature of maximum combustion rate (T_{MAX}) taken from the derivative of the TGA curve. These values give an indication of the rate of oxidation and the purity and uniformity of the samples.

It is well documented that oxidation temperature relates to residual catalyst and defects present in the structure of carbon nanotubes [56]. From the Raman analysis it was shown that all powders are similar in terms of defects with all having relatively high levels. MWNTs from Bayer combust at a lower temperature than those from Nanocyl™, with NC7000 and C150P having T_{MAX} of 579 °C and 543 °C respectively. This can be seen more clearly in Fig. 12. For both manufacturers, purification increases oxidation temperature but the increase in T_{MAX} is larger for Bayer than for Nanocyl™ nanotubes; NC7000 to NC3100 has an increase in T_{MAX} of 19 °C where C150P to C150HP has an increase of 38 °C. Although the residual catalyst for NC7000 is higher than all other samples, EDX has shown that the majority of that is aluminium oxide catalyst support rather than metal catalyst particles. For C150P, more of

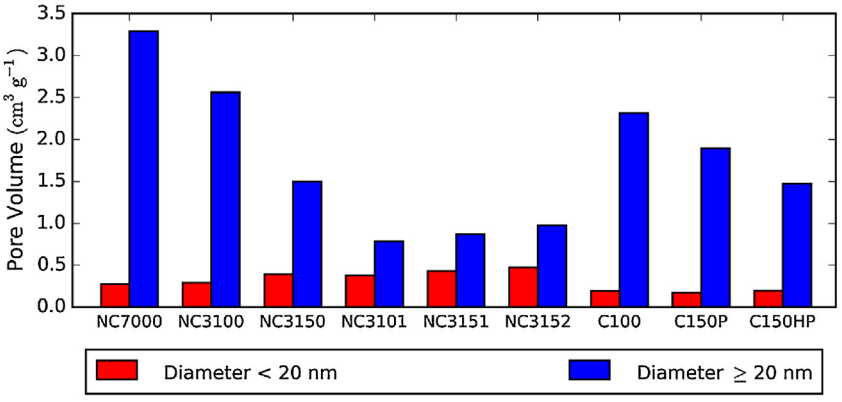

Fig. 11. Pore volumes for each distribution showing a decrease in volume with further processing.

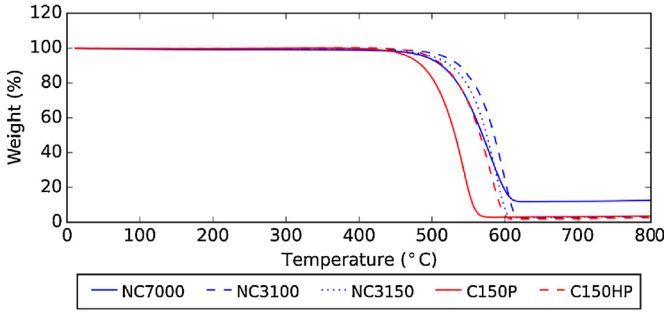

Fig. 12. Thermal decomposition of MWNTs.

the residual is metal catalyst (manganese and cobalt), which would explain the lower oxidation temperature. C100 oxidises at a temperature much closer to that of NC7000 than that of C150P even though C100 does have a large amount of residual iron catalyst.

The EDX analysis for C100 indicated no cobalt catalyst and both NC7000 and C150P use cobalt as a co-catalyst with C150P showing higher amounts than NC7000, which implies that the oxidation temperature is more affected by the amount of residual cobalt in the samples than residual support material or iron. For the further processed Nanocyl™ grades, there is a reduction in T_{MAX} of 10 °C from NC3100 to NC3150, which is likely caused by the increase in tube ends and increase in accessible surface area shown by nitrogen sorption data. Functionalised grades show a drop in mass below 300 °C, which is the oxidation of the functional groups [57], leaving exposed defects and hotspots reducing the T_{MAX} by 80 °C and 100 °C for NC3101 and NC3151 from their un-functionalised equivalents.

5. Concluding discussion

It is shown by SEM that the agglomerate structure of industrial MWNTs from Nanocyl™ (NC7000) take the form of highly entangled ropes or yarns of individual tubes, which then tangle to form large agglomerates. Industrial grade MWNTs from Arkema (C100) and Bayer (C150P) are similar to each other, taking the form of tightly entangled bundles, but there is no sign of the alignment present in the NC7000. The more aligned and likely longer tubes of NC7000 should lead to lower percolation thresholds than the other commercial grades studied when properly dispersed in coatings or composites.

EDX suggests that differences in structure of the agglomerates come from differences in growth conditions, with NC7000 being grown from platelets of aluminium oxide, while those of C100 and C150P are grown from a support that disintegrates as the tubes grow. EDX confirms the catalysts and support used during growth and shows that although NC7000 has the highest level of impurities, the majority is aluminium oxide support rather than transition metal catalyst. The high level of catalyst, as well as being shown to affect the thermal properties of the MWNTs, will also have to be considered when incorporating MWNTs in resin systems. The relatively large support platelets of aluminium oxide observed in NC7000 will be present in any cured resin system and must be stabilised. The small sizes of the disintegrated catalyst support of C100 and C150P will likely have little effect on the coating or composite they are dispersed into. If the aluminium oxide particles of NC7000 do give undesired properties to cured resin systems, the purified grade (NC3100) would be a good alternative.

Raman spectroscopy gives similar D/G and 2D/G ratios implying all grades are similar to each other in terms of quality. There is no indication that the purification processes used by Nanocyl™ or Bayer MaterialScience, or the functionalisation process used by Nanocyl™, increase the number of defects within the nanotubes.

TGA shows a higher thermal stability for Nanocyl™ grades when compared to Arkema or Bayer and this is thought to be due to the higher level of residual transition metal catalyst in the latter samples. TGA and EDX also confirmed the purified grades from Nanocyl™ (NC3100) and Bayer (C150HP) contain lower levels of residual catalyst and that the purification process appears more effective on the catalyst support than the transition metal catalyst itself. These differences in thermal stability could cause different changes in the thermal stability of any coating they are dispersed into. These results also highlight thermal stability is not always directly related to purity and that an understanding of the nature of any impurities is important.

A tightening of the agglomerate structures during processing, seen by SEM, is confirmed using BET and NLDFT and shows massive decreases in the volume of the larger pores, attributed to the agglomerate structure, following wet chemical treatment. As a result, an indication of agglomerate structure can be obtained on a larger sample size using BET and NLDFT than with SEM.

XPS shows that all grades have a low concentration of oxygen on the surface from the CVD growth process and that COOH functionalised grades from Nanocyl™ (NC3101 and NC3151) have increases of circa 10% oxygen on their surfaces. This functional surface should lead to better compatibility and stability in specific resin systems.

6. Conclusions

Commercially CVD grown MWNTs are supplied with various agglomerate structures and these structures are dependent on the growth mechanisms used. Wet processing of MWNTs changes agglomerate structure and leads to a tightening of the MWNT bundles. Residual catalyst left from nanotube growth has an effect on the thermal stability of the MWNT powder, with residual transition metal having a larger impact on oxidation temperature than the support material. All samples investigated in this body of work were shown to be of similar quality with regards to crystallinity.

Acknowledgements

This research was supported by the Engineering and Physical Science Research Council (EPSRC) through the Centre for Doctoral Training (CDT) in Micro- and NanoMaterials and Technologies (MiNMaT) at the University of Surrey and Indestructible Paint Ltd [EPSRC Grant reference number: EP/G037388/1].

References

[1] S. Iijima, Helical microtubules of graphitic carbon, Nature 354 (6348) (1991) 56–58.
[2] J.N. Coleman, U. Khan, W.J. Blau, Y.K. Gun'ko, Small but strong: a review of the mechanical properties of carbon nanotube–polymer composites, Carbon 44 (9) (2006) 1624–1652.
[3] Y. Ando, X. Zhao, H. Shimoyama, G. Sakai, K. Kaneto, Physical properties of multiwalled carbon nanotubes, Int. J. Inorg. Mater. 1 (1) (1999) 77–82.
[4] M.K. Samani, N. Khosravian, G.C.K. Chen, M. Shakerzadeh, D. Baillargeat, B.K. Tay, Thermal conductivity of individual multiwalled carbon nanotubes, Int. J. Therm. Sci. 62 (0) (2012) 40–43.
[5] I. O'Connor, S. De, J.N. Coleman, Y.K. Gun'ko, Development of transparent, conducting composites by surface infiltration of nanotubes into commercial polymer films, Carbon 47 (8) (2009) 1983–1988.
[6] A. Beigbeder, R. Mincheva, M.E. Pettitt, M.E. Callow, J.A. Callow, M. Claes, P. Dubois, Marine fouling release silicone/carbon nanotube nanocomposite coatings: on the importance of the nanotube dispersion state, J. Nanosci. Nanotechnol. 10 (5) (2010) 2972–2978.
[7] J. Liu, R. Liu, Y. Yuan, S. Zhang, X. Liu, Preparation of superhydrophobic antistatic coatings from branched alternating copolymers P(St-alt-MAn) and carbon nanotubes based on organic–inorganic hybrid approach, Prog. Org. Coat. 76 (9) (2013) 1251–1257.
[8] I.D. Rosca, S.V. Hoa, Highly conductive multiwall carbon nanotube and epoxy composites produced by three-roll milling, Carbon 47 (8) (2009) 1958–1968.
[9] Z. Dang, K. Shehzad, J. Zha, A. Mujahid, T. Hussain, J. Nie, C. Shi, Complementary percolation characteristics of carbon fillers based electrically

percolative thermoplastic elastomer composites, Compos. Sci. Technol. 72 (1) (2011) 28–35.
[10] Z. Wen, Q. Wang, Q. Zhang, J. Li, In situ growth of mesoporous SnO_2 on multiwalled carbon nanotubes: a novel composite with porous-tube structure as anode for lithium batteries, Adv. Funct. Mater. 17 (15) (2007) 2772–2778.
[11] L. Yuan, H. Yuan, X. Qiu, L. Chen, W. Zhu, Improvement of cycle property of sulfur-coated multi-walled carbon nanotubes composite cathode for lithium/sulfur batteries, J. Power Sources 189 (2) (2009) 1141–1146.
[12] L. Shen, C. Yuan, H. Luo, X. Zhang, K. Xu, F. Zhang, In situ growth of $Li_4Ti_5O_{12}$ on multi-walled carbon nanotubes: novel coaxial nanocables for high rate lithium ion batteries, J. Mater. Chem. 21 (3) (2011) 761–767.
[13] A.S. Brady-Estévez, M.H. Schnoor, C.D. Vecitis, N.B. Saleh, M. Elimelech, Multiwalled carbon nanotube filter: improving viral removal at low pressure, Langmuir 26 (18) (2010) 14975–14982.
[14] J. Tessonnier, D. Rosenthal, T.W. Hansen, C. Hess, M.E. Schuster, R. Blume, F. Girgsdies, N. Pfänder, O. Timpe, D.S. Su, R. Schlögl, Analysis of the structure and chemical properties of some commercial carbon nanostructures, Carbon 47 (7) (2009) 1779–1798.
[15] B. Krause, M. Mende, P. Pötschke, G. Petzold, Dispersability and particle size distribution of CNTs in an aqueous surfactant dispersion as a function of ultrasonic treatment time, Carbon 48 (10) (2010) 2746–2754.
[16] F. Liu, X. Zhang, J. Cheng, J. Tu, F. Kong, W. Huang, C. Chen, Preparation of short carbon nanotubes by mechanical ball milling and their hydrogen adsorption behavior, Carbon 41 (13) (2003) 2527–2532.
[17] Y. Feng, H. Zhang, Y. Hou, T.P. McNicholas, D. Yuan, S. Yang, L. Ding, W. Feng, J. Liu, Room temperature purification of few-walled carbon nanotubes with high yield, ACS Nano 2 (8) (2008) 1634–1638.
[18] V. Datsyuk, M. Kalyva, K. Papagelis, J. Parthenios, D. Tasis, A. Siokou, I. Kallitsis, C. Galiotis, Chemical oxidation of multiwalled carbon nanotubes, Carbon 46 (6) (2008) 833–840.
[19] J.-H. Ahn, H.-S. Shin, Y.-J. Kim, H. Chung, Structural modification of carbon nanotubes by various ball milling, J. Alloys Compd. 434–435 (2007) 428–432.
[20] S.A. Nanocyl, NANOCYL™ NC7000 series – Product Datasheet – Thin Multi-Wall Carbon Nanotubes (10 March 2009 – V05).
[21] Nanocyl S.A., NANOCYL™ NC3100 series - Product Datasheet – Thin Multi-Wall Carbon Nanotubes (10 March 2009 – V03).
[22] S.A. Nanocyl, NANOCYL™ NC3150 series – Product Datasheet – Short Thin Multi-Wall Carbon Nanotubes (10 March 2009 – V03).
[23] Arkema, Graphistrengh® C100 Technical Data Sheet (September 2008 – Rev. 4).
[24] Bayer MaterialScience AG, Baytubes® C150P Data Sheet (2010–07–05).
[25] Bayer MaterialScience AG, Baytubes® C150HP Data Sheet (2008–11–13).
[26] S. Brunauer, P.H. Emmett, E. Teller, Adsorption of Gases in multimolecular Layers, J. Am. Chem. Soc. 60 (2) (1938) 309–319.
[27] P. Tarazona, Free-energy density functional for hard spheres, Phys. Rev. A 31 (4) (1985) 2672–2679.
[28] P. Tarazona, U.M. Marconi, R. Evans, Phase equilibria of fluid interfaces and confined fluids, Mol. Phys. 60 (3) (1987) 573–595.
[29] C.H. See, A.T. Harris, A review of carbon nanotube synthesis via fluidized-bed chemical vapor deposition, Ind. Eng. Chem. Res. 46 (4) (2007) 997–1012.
[30] M.J. Becker, W. Xia, J. Tessonnier, R. Blume, L. Yao, R. Schlögl, M. Muhler, Optimizing the synthesis of cobalt-based catalysts for the selective growth of multiwalled carbon nanotubes under industrially relevant conditions, Carbon 49 (15) (2011) 5253–5264.
[31] A. Dupuis, The catalyst in the CCVD of carbon nanotubes—a review, Prog. Mater. Sci. 50 (8) (2005) 929–961.
[32] A. Magrez, J.W. Seo, R. Smajda, M. Mionić, L. Forró, Catalytic CVD synthesis of carbon nanotubes: towards high yield and low temperature growth, Materials 3 (11) (2010) 4871–4891.
[33] R.P. Silvy, Method of Synthesising a Support Catalyst for the Production of Carbon Nanotubes, Patent 20080213160 (2008).
[34] R.P. Silvy, Catalyst System for a Multi-Walled Carbon Nanotube Production Process, Patent 20080206125 (2008).
[35] H. Hocke, Carbon Nanotube Agglomerate, Patent 20120149824 (2012).
[36] H. Hocke, R. Weber, O.F.-k. Schlüter, V. Michele, L. Mileczko, Production Of Carbon Nanotubes, Patent 20130039839 (2013).
[37] S. Bordere, Method For Synthesis Of Carbon Nanotubes, Patent 20090134363 (2009).
[38] M. Pumera, Carbon nanotubes contain residual metal catalyst nanoparticles even after washing with nitric acid at elevated temperature because these metal nanoparticles are sheathed by several graphene sheets, Langmuir 23 (11) (2007) 6453–6458.
[39] Q. Zhang, J. Huang, M. Zhao, W. Qian, F. Wei, Carbon nanotube mass production: principles and processes, ChemSusChem 4 (7) (2011) 864–889.
[40] M. Bierdel, S. Buchholz, V. Michele, L. Mleczko, R. Rudolf, M. Voetz, A. Wolf, Industrial production of multiwalled carbon nanotubes, Phys. Status Solidi B 244 (11) (2007) 3939–3943.
[41] G. Atthipalli, H. Wang, J.L. Gray, Catalyst-assisted vertical growth of carbon nanotubes on Inconel coated commercial copper foil substrates versus sputtered copper films, Appl. Surf. Sci. 273 (0) (2013) 515–519.
[42] D.T. Clark, B.J. Cromarty, A. Dilks, A theoretical investigation of molecular core binding and relaxation energies in a series of oxygen-containing organic molecules of interest in the study of surface oxidation of polymers, J. Polym. Sci.: Polym. Chem. Ed. 16 (12) (1978) 3173–3184.
[43] D.T. Clark, H.R. Thomas, Applications of ESCA to polymer chemistry. XVII. Systematic investigation of the core levels of simple homopolymers, J. Polym. Sci.: Polym. Chem. Ed. 16 (4) (1978) 791–820.
[44] M.S. Dresselhaus, G. Dresselhaus, R. Saito, A. Jorio, Raman spectroscopy of carbon nanotubes, Phys. Rep. 409 (2) (2005) 47–99.
[45] A. Ferrari, J. Meyer, V. Scardaci, C. Casiraghi, M. Lazzeri, F. Mauri, S. Piscanec, D. Jiang, K. Novoselov, S. Roth, Raman spectrum of graphene and graphene layers, Phys. Rev. Lett. 97 (18) (2006) 187401.
[46] K. Behler, S. Osswald, H. Ye, S. Dimovski, Y. Gogotsi, Effect of thermal treatment on the structure of multi-walled carbon nanotubes, J. Nanopart. Res. 8 (5) (2006) 615–625.
[47] R.A. DiLeo, B.J. Landi, R.P. Raffaelle, Purity assessment of multiwalled carbon nanotubes by Raman spectroscopy, J. Appl. Phys. 101 (6) (2007) 064307.
[48] A. Eckmann, A. Felten, A. Mishchenko, L. Britnell, R. Krupke, K.S. Novoselov, C. Casiraghi, Probing the nature of defects in graphene by Raman spectroscopy, Nano Lett. 12 (8) (2012) 3925–3930.
[49] Y. Wang, D.C. Alsmeyer, R.L. McCreery, Raman spectroscopy of carbon materials: structural basis of observed spectra, Chem. Mater. 2 (5) (1990) 557–563.
[50] C. Deng, W. Lin, S. Eimer, D. Ravelosona, C. Chappert, W. Zhao, Raman spectroscopy study of low energy He^+ ion irradiation effect in graphene transferred onto SiO_2, in: 2013 13th IEEE Conference on Nanotechnology IEEE-NANO, 2013, pp. 903–906.
[51] H. Cui, G. Eres, J.Y. Howe, A. Puretkzy, M. Varela, D.B. Geohegan, D.H. Lowndes, Growth behavior of carbon nanotubes on multilayered metal catalyst film in chemical vapor deposition, Chem. Phys. Lett. 374 (3–4) (2003) 222–228.
[52] K.S. Sing, Reporting physisorption data for gas/solid systems with special reference to the determination of surface area and porosity (Recommendations 1984), Pure Appl. Chem. 57 (4) (1985) 603–619.
[53] J. Rouquerol, D. Avnir, C. Fairbridge, D. Everett, J. Haynes, N. Pernicone, J. Ramsay, K. Sing, K. Unger, Recommendations for the characterization of porous solids (Technical Report), Pure Appl. Chem. 66 (8) (1994) 1739–1758.
[54] A. Peigney, C. Laurent, E. Flahaut, R. Bacsa, A. Rousset, Specific surface area of carbon nanotubes and bundles of carbon nanotubes, Carbon 39 (4) (2001) 507–514.
[55] X. Ling, Y. Wei, L. Zou, S. Xu, The effect of different order of purification treatments on the purity of multiwalled carbon nanotubes, Appl. Surf. Sci. 276 (0) (2013) 159–166.
[56] J.H. Lehman, M. Terrones, E. Mansfield, K.E. Hurst, V. Meunier, Evaluating the characteristics of multiwall carbon nanotubes, Carbon 49 (8) (2011) 2581–2602.
[57] R. Yudianti, H. Onggo, Y.S. Sudirman, T. Iwata, J. Azuma, Analysis of functional group sited on multi-wall carbon nanotube surface, Open Mater. Sci. J. 5 (2011) 242–247.